


Method of automatic calibration and measurement of the light polarisation plane rotation with tilted fibre Bragg gratings and discrete wavelet transform usage

Marta Dziuba-Kozieł^{1*} , Grzegorz Kozieł¹, Damian Harasim¹,
Piotr Kisała¹, Marcin Kochanowicz²

¹ Faculty of Electrical Engineering and Computer Science, Lublin University of Technology, ul. Nadbystrzycka 38A, 20-618 Lublin, Poland

² Faculty of Electrical Engineering, Białystok University of Technology, ul. Wiejska 45D, 15-351 Białystok, Poland

* Corresponding author's e-mail: g.koziel@pollub.pl

ABSTRACT

Fibre optic sensors are used to measure various physical quantities, including polarisation plane rotation. Existing solutions for measuring the rotation of the plane of polarisation in optical fibres are based on sensors using tilted fibre Bragg gratings (TFBGs). Articles describing the possibilities of measuring the rotation of the plane of polarisation are generally concepts that show the effect of the rotation of the plane of polarisation on quantities such as the change in optical power of the light transmitted through the TFBG, or the change in the position of the selected minimum of the light spectrum. The only method that allows the measurement of the rotation of the plane of polarisation bases on optical spectrum analysis and requires manual calibration by an experienced operator. The paper proposes a fully automatic method of sensor calibration and processing the signal from a TFBG to measure the light polarisation plane rotation. The method uses the discrete wavelet transform (DWT) to process the light spectrum. An automatic algorithm to choose optimal DWT coefficients to use has been developed. The presented method offers calibration of light polarisation plane rotation angle sensors avoiding the influence of manufacturing imperfections of the measurement system components. In addition, it allows the calibration process to be fully automated without operator involvement. The developed measurement method is also fully automated. It allows measurement of angles of rotation in the range of 0–180, making it possible to distinguish between 0–90 and 90–180 rotation angle ranges without any problems. The mean square error of measurement over the entire range is 0.37 degrees, which is better than that of competing methods. In addition, an independent measurement method operating in the 82–98 rotation angle range is proposed to increase measurement precision in this range.

Keywords: TFBG, polarisation, DWT, rotation, measurement, fibre, Bragg, optic.

INTRODUCTION

Fibre optic sensors are used where other types of sensors fail. This is due to their immunity to interference and lack of interference introduced to the environment. Other features are also important. Fibre optic sensors are used in environments with significant levels of radiation [1]. Among other things, this allows them to be used in space. Also, lightweight and small size are important arguments for their use in space and aerospace solutions [2]. They are made of glass and can be

used in high-voltage measurement systems [3, 4] For the same reason, fibre optic sensors can be used in liquids [5]. The high resistance of glass against temperature allows the creation of temperature sensors to work in high temperatures [6, 7]. Their important advantage is insensitivity to electromagnetic fields [8]. They can work in high-pressure environments [9]. Also, hazardous or explosive substances are not a problem [10, 11]. The important aspect that often makes constructors use fibre-optic sensors is their mechanical strength, resistance to corrosion, reliability and repeatability

of measurements [12]. Apart from the above, fibre optic sensors do not introduce interference to the environment, making them ideal sensors in applications where interference can be harmful. It is also important that optic fibre parameters can be easily measured and controlled [13, 14].

Bragg gratings inside optic fibre structures make them sensitive to various physical quantities. Multiple types of gratings can be distinguished. Most of them are created by fringes positioned perpendicular to the fibre axis. Such structures are sensitive to temperature and pressure because of the change in distance between fringes [15, 16]. They are sensitive to fibre bending and vibration, which changes the angle between fringes [17, 18]. Positioning grating fringes at the angle to the cross-section plane of the fibre leads to the creation of tilted fibre Bragg gratings (TFBGs). TFBGs reflect some of the light to the cladding, creating cladding modes [19]. Light propagating in the cladding partially disperses in the surroundings and makes TFBGs sensitive to the environment parameters [20]. Covering TFBGs with coatings makes them sensitive to the presence of some substances [19, 21]. TFBGs also offer possibilities for analysing the properties of light propagating inside the fibre. One such possibility is sensing the angle of light polarisation plane rotation.

In the paper, a novel method of light polarisation plane rotation measurement is presented. The proposed method, unlike others, offers automation of the manufacturing process of the light polarisation plane rotation angle sensor.

The results obtained allow the proposed method to be used in fibre optic measurement systems that are sensitive to changes in polarisation angle to control the angle. In addition, the proposed sensor can be used to monitor the tilt angle and rotation of moving components. It will find application in environments exposed to adverse factors such as radiation or electromagnetic fields, due to the insensitivity of optical fibres to these factors.

RELATED WORKS

There are only a few papers in the literature treating the measurement of the angle of light polarisation plane rotation. Sensors integrated into an optical fibre are in the early stages of development. In the paper [22], the possibility

of measuring the rotation angle of the plane of polarisation of light propagating in optical fibre was demonstrated and test measurements were made. In the system used by the authors, polarised light propagated through the TFBG and then through a circulator was directed to an optical fibre with a FBG. The FBG's task was to reflect a narrow range of light wavelengths, corresponding to the selected sheath mod of the TFBG grating used. The reflected light was directed through a circulator to a detector connected to an optical power meter. In the case discussed, a mod containing light with wavelengths in the range 1520.6–1520.9 nm, which responds strongly to a change in the angle of light polarisation plane rotation, was selected for analysis. The authors present the results of measurements in the angles range of 0–180 with a resolution of 9°. It is evident that the measured optical power decreases when changing the rotation angle in the range of 0–90 and then increases in the range of 90–180. The authors indicate that the change in power in the angles ranges 25–65 and 115–155 is quasi-linear. They argue that it is impossible to distinguish between the ranges 25–65 and 115–155 when measurements are made using the method discussed above.

Paper [23] presents a study demonstrating the possibility of measuring the angle of light polarisation plane rotation by monitoring changes in the value of the light transmission coefficient for a single wavelength. In the example presented, it was a wavelength of 1541.2 nm. The wavelength tested was not chosen at random but corresponds to the location where the P-type mod occurs for the TFBG grating used and its value changes significantly when the angle of light polarisation plane rotation changes.

In this study, a measurement system was used, consisting of a light source in the form of an SLD superluminescent diode, from which light was sent to a polariser and half-waveguide via an optical fibre and lens. The light was then sent to a TFBG with a tilt angle of periodic structures of $\Theta=6^\circ$, from which it went to an optical spectrum analyser.

The authors performed two series of measurements with a resolution of 10°. One involved the rotation angle of the fibre with the TFBG mesh from 0–90 to the right. The second series involved the rotation of the fibre with the TFBG mesh from 0–90 to the left. In this way, the authors measured a rotation with a total range of 180°. Based on the measurements, a processing

characteristic of the periodic structure under study was created. The authors indicate that their study confirms the occurrence of changes in the transmission of light for the wavelength under study as a function of the light polarisation plane rotation. It was also determined that the present method offers maximum sensitivity in the angles range of 30-70 and the nature of the changes is the same for both right and left-hand rotation. The method in question thus allows changes in the angle of rotation of the plane of polarisation of light to be detected. However, it does not provide the ability to distinguish which way the TFBG has been rotated.

The most mature method of light polarisation plane rotation angle measurement is presented in [24]. The measurement is done by the analysis of the TFBG transmission spectrum. The proposed sensor has to be calibrated before usage. Measurement is taken with an optical spectrum analyser. The obtained spectrum is transformed with the Fourier transform. The angle of rotation is calculated by analysing the value of these Fourier transform coefficients for whose characteristics were created in a calibration process. Calibration is necessary to create chosen coefficients characteristics. The issue with the calibration process is the need for an experienced technician who is responsible for choosing the characteristics to use. The reported method can measure the angle of light polarisation plane rotation in the angles range from 0 to 180. The average measurement error reported in [24] is 1,5°. Authors indicate that the method is characterised by an increased level of error for rotation angles close to 0, 45, 90, 135 and 180. They also report issues with the method at the boundaries of the measurement range – near 0 and 180 degrees.

MATERIALS AND METHODS

Measurement set

The measurement set consists of a light source, a polariser, collimators and a half-wave-length plate, behind which a splitter is placed. The splitter splits the light into two parts, one of them is directed to the TFBG and then to the optical spectrum analyser (OSA). The other part is sent to the second spectrum analyser. A schema of the measurement set is shown in Figure 1.

The measurement set was constructed so that linearly polarised light could be sent to the input of the TFBG. Moreover, the possibility of changing the angle of light polarisation plane rotation at the input of the grating was provided. Measurement of the grating response was realised by connecting the grating output with the input of the OSA. An additional assumption was to minimise the influence of additional devices included on the measurement result. Therefore, before the TFBG a splitter was placed, to which an additional OSA was connected. This made it possible to monitor changes in the signal applied to the input of the TFBG grating. To avoid temperature influence on the measurement, the fibre optic element containing the TFBG was placed in a climate chamber at a stabilised temperature of 24 degrees Celsius. The light source in the measurement system was a superluminescent diode – Thorlabs S5FC1550S-A2 (SLD). It is equipped with a low-noise DC source and a temperature control unit to ensure stable performance.

A light polarisation plane angle control unit was connected to the light source via a fibre optic cable. This consisted of a Thorlabs CFP2-1550A collimator placed to create a parallel beam of light propagating through the air. Behind the

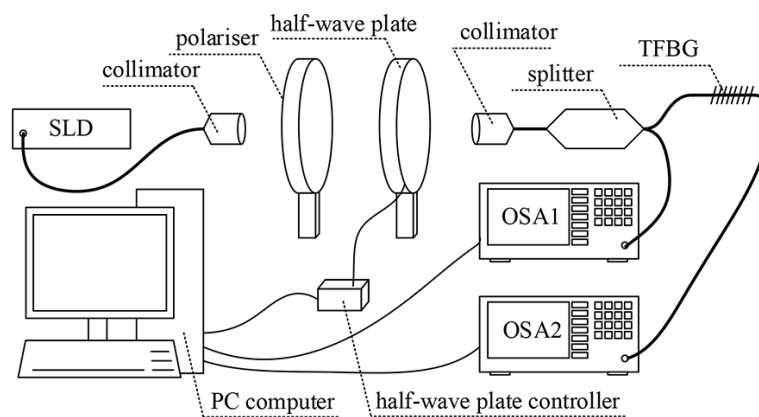


Figure 1. Measurement set schema

collimator, a polariser was placed. The polariser was aligned with input light polarisation. Next, in the path of the light beam, a Thorlabs WPHSM05-1550, electronically-controlled half-wave plate was placed, providing 0.1° of rotational angle precision. It was used to control the angle of rotation of the light polarisation plane. The light coming out of the half-wave plate reached to a second Thorlabs CFP2-1550A collimator, which focused the light and directed it into the optical fibre. This collimator was mounted on a three-axis table allowing positioning of the collimator in three dimensions.

Behind the collimator, a 1x2 splitter was placed with a claimed light split of 50:50. A Yokogawa AQ6730D spectrum analyser was connected to the first output of the splitter. It was used to measure the spectrum of the light fed into the TFBG, which was connected to the second output of the splitter. A second Yokogawa AQ6730D spectrum analyser was connected to the TFBG output. It measured the spectrum of light propagating through the TFBG. A TFBG with a tilt angle of 7° was used.

The measurement set was placed on a Thorlabs Nexus optical table, which was used to eliminate vibrations and provide mounting holes for fixing the system components.

Measurements

Before starting the measurements, all devices in the measurement set were switched on. The collimators and polariser were positioned to obtain the maximum light output of the measurement system. This was done by moving the collimators in three axes and rotating the polariser. The devices were left on for an hour to stabilise their operating conditions. The temperature in the climate chamber was also stabilised. The initial rotation angle of the light polarisation plane was set to 0° relative to the fibre cross-section. The half-wave plate rotation angle was then changed by half a degree and another measurement was taken. This resulted in a 1° change in the angle of the light polarisation plane. This operation was repeated until all measurements in the series had been made – the plane of light polarisation was rotated by 180° .

During the measurements, light spectra were recorded with OSA1 and OSA2 analysers. As they do not provide the possibility to perform measurements automatically and simultaneously, they were initiated manually by pressing the buttons of

both recorders. To eliminate the influence of elements of the light polarisation plane rotation angle control system and the light source, the spectra obtained from the OSA2 analyser were divided by the corresponding spectra obtained from the OSA1. The dividing operation results were considered the final measurement result and subjected to further numerical analysis to calculate the measured light polarisation plane rotation angle.

Discrete wavelet transform

The discrete wavelet transform (DWT) derives from the Fourier transform, which is a powerful tool used in many applications [25, 26]. It can be applied in engineering, medicine and other domains to analyse various signal artefacts [27, 28]. The Fourier transform does not give a possibility of obtaining good time resolution contrary to the DWT [29]. The DWT is useful in the analysis of transients and waveforms characterised by high variability. The spectrum of light propagating through a TFBG has such a characteristic. If we treat a single spectrum or part of it as a signal, we can process it using a wavelet transform.

A wavelet transform is a signal transformation that allows its analysis to be performed. A time-frequency analysis is performed for signals represented in the time domain [25]. The discrete wavelet transform is described by the formula:

$$a_{m,n} = \sum x(t) \psi_{m,n}(t) \quad (1)$$

where: $x(t)$ is the signal to be analysed, $\psi(t)$ is the mother wavelet, and m, n are integers. In the case of light spectra, the analysis will be carried out in the wavelength and frequency domains.

In the discrete wavelet transform process, the signal is analysed using a mother wavelet, which is moved along the signal to be analysed. Its correlation with the corresponding signal part is determined, resulting in a transform coefficient. Once the whole signal has been analysed, its representation in the form of a series of coefficients is obtained. This series consists of two parts: approximation and details. The details contain the high-frequency components of the signal, while the approximation contains a low-frequency representation of the signal. The approximation can again be subjected to a wavelet transform, obtaining results at the next level of decomposition. The

wavelet transform can be represented as a decomposition tree shown in Figure 2. The higher the decomposition level, the coarser the signal features it represents.

The automatic method of wavelets and their decomposition levels choose

In the proposed method, the calculation of the measured rotation angle is performed by analysing the values of the sum of the coefficients at selected levels of the DWT decomposition calculated using the selected mother wavelets. Due to differences in the internal structure of the TFBGs, the results obtained for different gratings may vary. Therefore, a method has been developed for the selection of wavelets and decomposition levels to be used in the calculations carried out. The proposed measurement system has to be calibrated. Calibration consists of measuring the angle of light polarisation plane rotation in the range $\alpha \in \langle 0, 180 \rangle$, optimally with a resolution of not less than 2° . The rotation angle has to be known when taking measurements in the calibration process. The spectra obtained from the measurements are processed with a wavelet transform using various wavelets ψ at different decomposition levels n . For each rotation angle α_k , the $X_{sum}(\psi, n, \alpha_k)$ coefficient values for each wavelet and each decomposition level are calculated independently. From these, vectors of values $W(\psi, n) = X_{sum}(\psi, n, \alpha_0), \dots, X_{sum}(\psi, n, \alpha_k), \dots, X_{sum}(\psi, n, \alpha_K)$ are created. Each vector $W(\psi, n)$ is then approximated by a polynomial regression $R(\psi, n)$ with a six-degree polynomial function. The mean squared error (*MSE*) of the approximation is calculated for each of the vectors. The vectors $W(\psi, n)$, for which the *MSE* was less than 10^{-5} , are used to calculate the rotation angle.

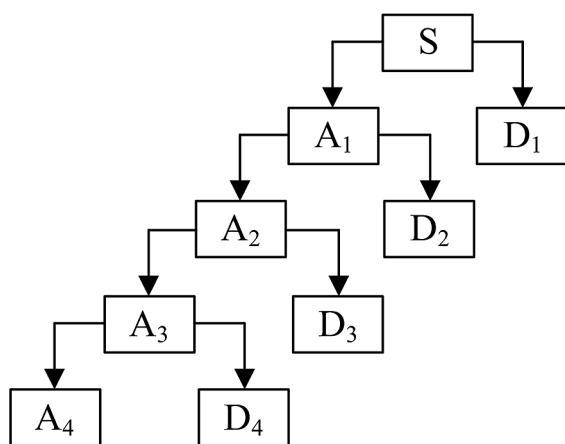


Figure 2. DWT decomposition tree

The result of the system calibration is a list of wavelets, decomposition levels and $W(\psi, n)$ vectors that will be used to determine the rotation angle. A block diagram of the algorithm for the automatic selection of wavelets and their decomposition levels is shown in Figure 3.

Calibration process

Achieving repeatability in the manufacturing process of Bragg gratings is difficult. It is also impossible to obtain identical measuring systems in the production process. Therefore, each measurement system has to be calibrated before use.

Calibration of the system consists of taking a series of measurements in the angles range $0-180^\circ$ of the angle of light polarisation plane rotation. Measurements should be taken with no more than 2° of rotation resolution. If higher resolutions are used, the accuracy of the measuring system may be lower. Additional limitations of the calibration process are that measurements must be taken for angles of rotation of $0, 90$ and 180 . For these rotation angles, there are maxima and minima of most functions used to determine the measured rotation angle. The spectra obtained from each measurement are processed by the DWT using selected wavelets. An independent transformation is performed for each mother wavelet. The result is a set of coefficients.

A set of vectors $W(\psi, n)$ is then created. Each vector consists of the sums of all the coefficients of the n^{th} level of the transform obtained for each rotation angle for which measurements were made during the calibration process. For the vectors obtained in this way, the noise level is evaluated as shown in Figure 4. The vectors $W(\psi, n)$ for which the evaluated distortion level (*MSE*) will be lower than 10^{-5} are stored in the measurement system memory. The $W(\psi, n)$ vectors, the wavelet name and the decomposition level used are saved in the set named FD_{cal} .

In addition, the calibration process identifies DWT coefficients characterised by significant value variation and low noise in the $\alpha \in 80-100$ range. For each DWT coefficient calculated from the spectra obtained during the calibration process, vectors (V) of values obtained for the measurements made during the calibration process are created. Each vector is then normalised so that its maximum value is one and the minimum is zero. The noise and slope of the normalised V_{norm} vectors are then examined in the range of rotation angles $\alpha \in 80-100$. For this purpose, a linear

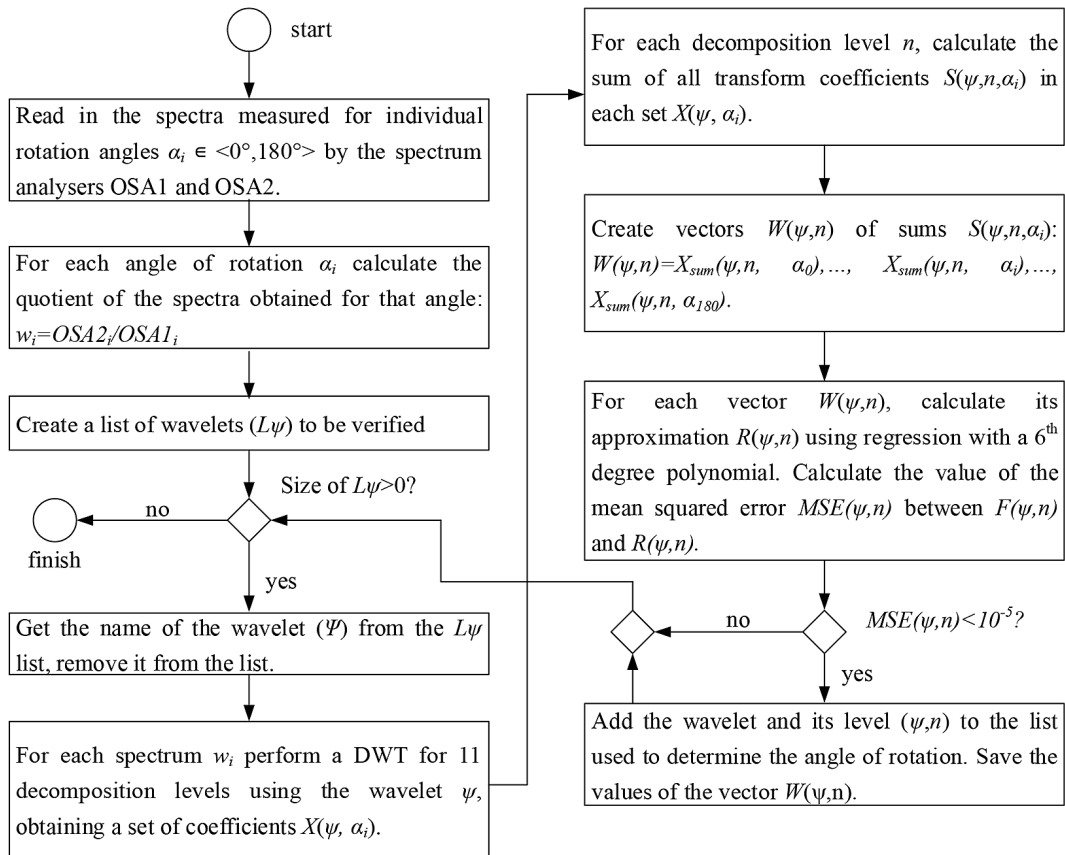


Figure 3. Diagram of the algorithm for the automatic selection of wavelets and their decomposition levels

regression model of each of the V_{norm} vectors in the range of rotation angles $\alpha \in 80-100$ is calculated. This takes the form $y=ax+b$. The coefficient a is taken as the slope of the tested waveform. Research conducted has shown that the coefficient varies in the range of -0.025 to 0.025 . Vectors whose absolute value of the coefficient a is greater than 0.018 are considered for further analysis.

Monotonic waveforms that are as close to rectilinear as possible are most useful due to the specifics of the application. For this reason, an algorithm has been developed to evaluate noise, based on changes examination in the angle of inclination of the segments connecting the individual points of the surveyed vector. The calculation is carried out according to the algorithm presented in Figure 4. The vectors V_{norm} of all DWT coefficients are evaluated in the presented manner. Of the vectors meeting the condition $a > 0.018$, 40 with the smallest noise coefficient value are selected. These are stored in the measurement system, in the set named W_{cal} , by saving for each of them the mother wavelet that was used to calculate the coefficient, its number and the part of vector V containing values in the range of rotation angles $\alpha \in 80-100$.

Rotation angle calculation

The spectrum of light measured with the calibrated system is subjected to a wavelet transform using each wavelet and each decomposition level from the set FD_{cal} . Sets of wavelet transform coefficients are obtained from which the mean values of $X_{sum}(\psi, n, \alpha_k)$ are calculated. Then the intersection points of the segments connecting the points of the vector $W(\psi, n)$ with the line $y = X_{sum}(\psi, n, \alpha_k)$ are determined. The angles of rotation α_k corresponding to these intersection points are read out, as shown in Figure 5. In this way, a set of α_k values is created, which forms the basis for further analysis. This set is denoted by the symbol K .

The values from the set K are divided into two subsets: K_I containing $\alpha_k \in <0,90>$, and K_{II} containing $\alpha_k \in <90, 180>$. Computed for the sets are:

- the numbers of elements in the sets: N_I denotes the number of values in the set K_I , N_{II} denotes the number of values in the set K_{II}
- mean values calculated according to the formulas:

$$\alpha_{Iavg} = \frac{\sum_{i=1}^{N_I} \alpha_k}{N_I} \tag{2}$$

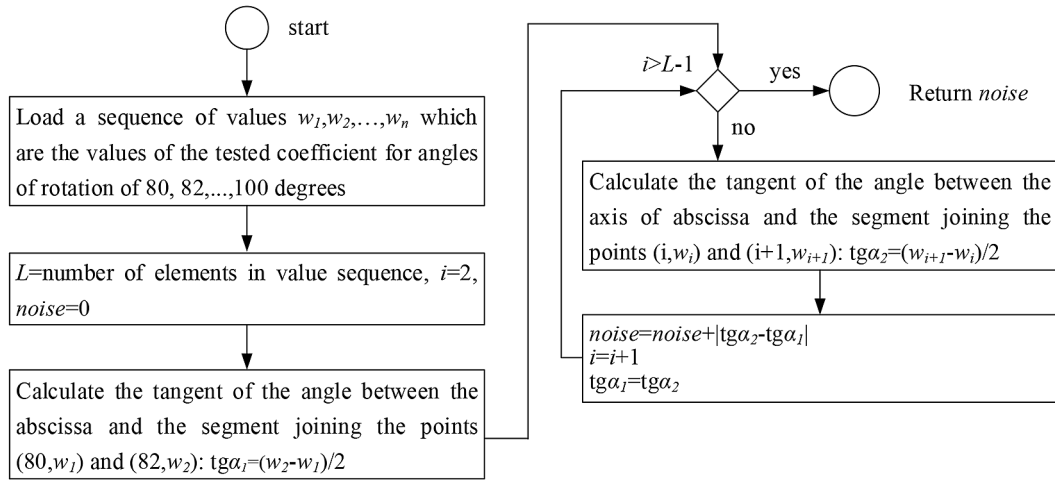


Figure 4. Diagram of the algorithm for the DWT coefficients noise assessment

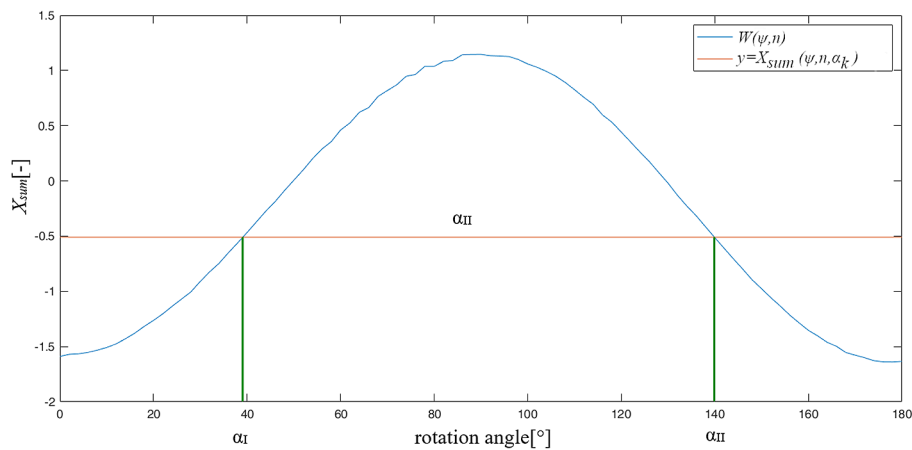


Figure 5. Reading rotation angles

$$\alpha_{IIavg} = \frac{\sum_{k=1}^{N2} \alpha_k}{N2} \quad (3)$$

where: α_k means the values of the angles in the sets, standard deviations of K_I and K_{II} calculated according to the formulas:

$$\sigma_I = \sqrt{\frac{\sum_{k=1}^{N1} |\alpha_k - \alpha_{Iavg}|^2}{N1}} \quad (4)$$

$$\sigma_{II} = \sqrt{\frac{\sum_{k=1}^{N2} |\alpha_k - \alpha_{IIavg}|^2}{N2}} \quad (5)$$

Due to the distribution of values in the $W(\psi, n)$ vectors, two rotation angle values are obtained for most measurements. They are usually distributed almost symmetrically to the rotation angle of 90° . Figure 6 shows a graph showing the values: α_{Iavg} and α_{IIavg} obtained for measurements made with a resolution of 1° of rotation. The values from the K_I set are close to the correct reading in the 0-90 range. For angles of rotation in the range of

90–180, a correct reading can be obtained by taking the value from the K_{II} set. The problem is the ambiguity of the reading – one of the two readings has to be selected.

The values α_{Iavg} and α_{IIavg} are average values calculated from the sets of K_I and K_{II} . To determine which value indicates the measured rotation angle, it is necessary to analyse the data from the sets K_I and K_{II} . This involves independently calculating the standard deviations and number of elements in each set. The research has shown that the standard deviation of the set whose mean value indicates the correct rotation angle is smaller – as shown in Figure 7. However, readings for angles α greater than 172 degrees cannot be correctly identified on this basis. In this case, it is necessary to analyse the number of elements in the K_I and K_{II} sets. It is noticeable that the number of values of the K_I set significantly decreases for angles of rotation greater than 172 degrees.

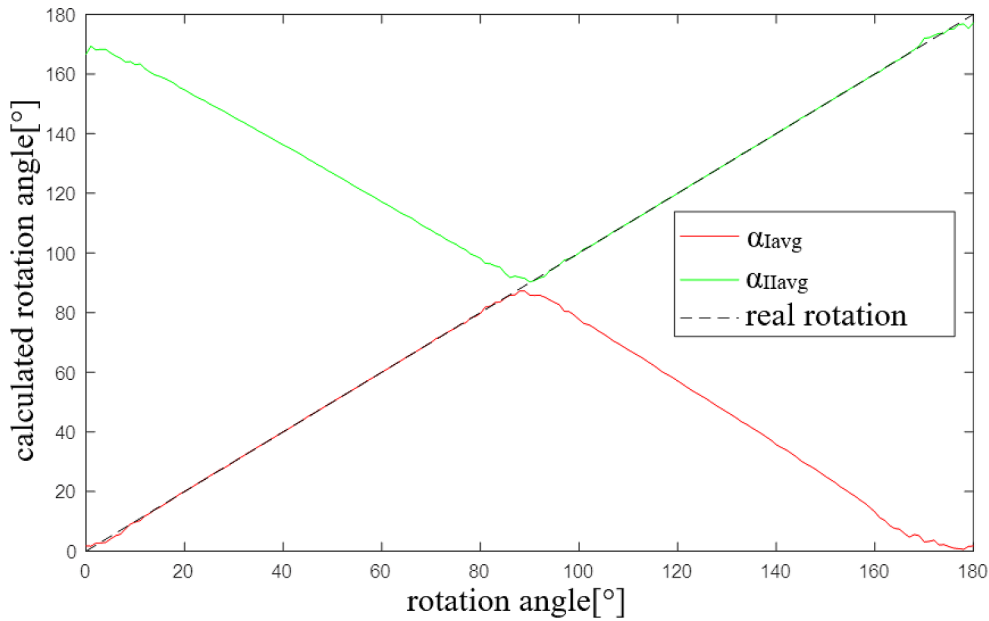


Figure 6. α_{lavg} and α_{llavg} values obtained for measurements made with a resolution of 1° of rotation

Therefore, when the calculated value of the rotation angle is in the range of 0–8 or 172–180, an analysis of the count of the K_l set is additionally performed. If the number of elements in this set is less than 50% of the number of vectors $W(\psi, n)$ then a value in the range 172–180 is taken as the measurement result, otherwise the result is a value in the range 0–8. A block diagram of the algorithm for calculating the measured rotation angle is shown in Figure 8.

In the solution presented, the problem remains the evaluation of the rotation angle in the range 86–94. The values of α_{lavg} and α_{llavg} are subject to error for $\alpha \in 86–94$. Recognition of this range of rotation angles is possible by analysing the values of α_{lavg} and α_{llavg} . Their functions in this range have a local minimum α_{llavg} and maximum α_{lavg} . Moreover, the difference in values between them is the smallest over the entire measurement range. However, evaluation based on the parameters mentioned is cumbersome and sometimes unreliable. If the result obtained is in the range of 82–98, a recalculation of the rotation angle is made by analysing the values of the selected DWT coefficients.

Recalculation of the measurement result in the case of obtaining a result between $\alpha \in 82$ and 98 is performed by analysing the values of the coefficients stored during calibration in the W_{cal} set. The value w of each of these coefficients is read, and then the angles of rotation corresponding to the intersection of the line $y=w$ with the function formed

by connecting the successive values of the analysed coefficient stored in the W_{cal} set by segments are read. From the set of read rotation angles, the 10% largest and 10% smallest values are removed to get rid of outliers. The average is calculated from the remainder, which is the result of the measurement. It is also possible that the algorithm will not be able to correctly calculate the rotation angle due to an insufficient number of coefficients in the W_{cal} set. Then it returns an error message. In this case, the previously estimated measurement value is left.

RESULTS AND DISCUSSION

Measurement results

To verify the developed method, measurements were made using gratings with tilt angles $\Theta = 5^\circ$ and $\Theta = 7^\circ$ of the TFBG structure. Before the measurements, the gratings were calibrated by taking measurements for angles $\alpha = 0, 2, 4, \dots, 180$. The following mother wavelets were used in the calibration process: void, bl7, coif5, dmey, bior1.5, han4.5, mb4.2 and mb4.4. Measurements were performed with a resolution of 1 degree in the range of 0–180 degrees of rotation. Measurement results obtained for the grating with $\Theta = 7^\circ$ are presented in Figure 9 and measurement inaccuracies for individual rotation angles are shown in Figure 10. Measurement results obtained for the grating with $\Theta = 5^\circ$ are presented in Figure 11 and

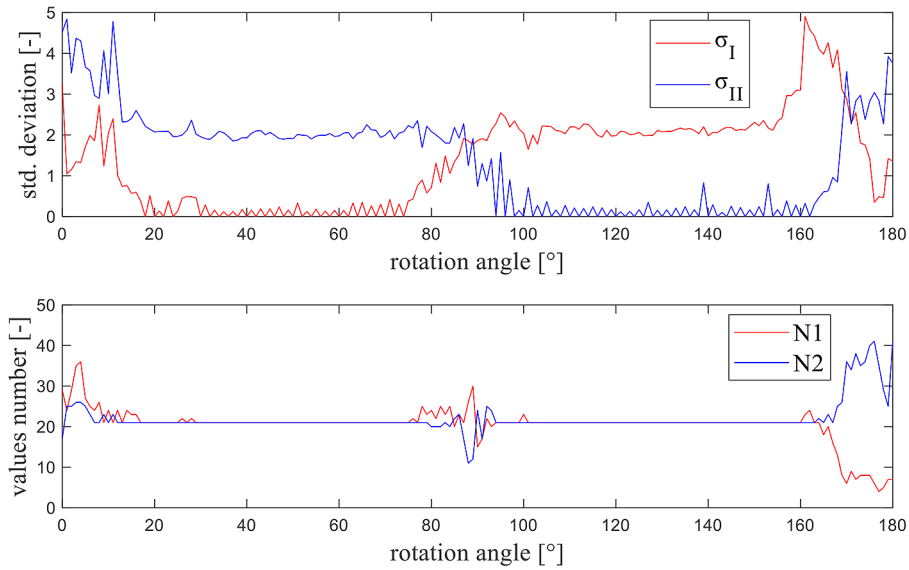


Figure 7. α_{Iavg} and α_{IIavg} values obtained for measurements made with a resolution of 1° of rotation

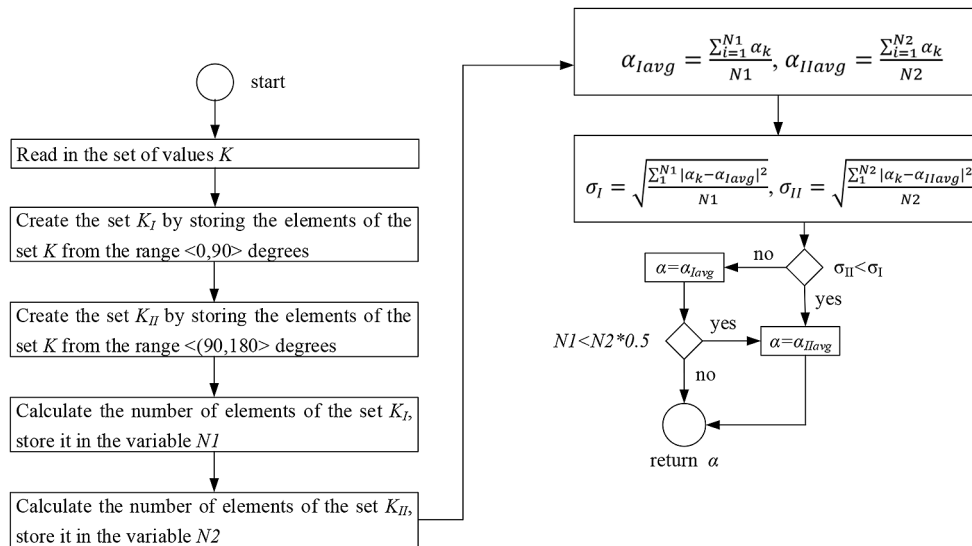


Figure 8. Diagram of the algorithm for calculating the measured rotation angle

its errors for individual rotation angles are shown in Figure 12. The average measurement error for a grating with $\theta = 7^\circ$ was $ME = 1.1^\circ$. For the grid with $\theta = 5^\circ$ $ME=1.5^\circ$. Analysis of the results revealed that the method offers the best measurement precision for rotation angles $\alpha \in (20, 70)$ and $\alpha \in (100, 160)$. This is because the functions $F(\psi, n)$ formed by connecting the points of the vectors $W(\psi, n)$ by segments have a significant slope in these ranges of rotation angles. In contrast, they flatten out in the other ranges. This significantly reduces the precision of the values reading causing an increased level of measurement error. The angle of tilt of the grating influences the results obtained. Increasing the tilt angle of structures

increases the precision of measurements. In the course of research, an attempt was made to construct a rotation angle sensor with a grating with a tilt angle $\theta = 3^\circ$. The results were unsatisfactory and, therefore, were not included in this study. Of the gratings tested, the best results were obtained for the one with $\theta = 7^\circ$. The grating with $\theta = 5^\circ$ generated a significantly bigger measurement error than the grating with $\theta = 7^\circ$.

Comparison to other solutions

The number of methods to measure the angle of rotation is small. The mechanisms for measuring the rotation angle of the light polarisation

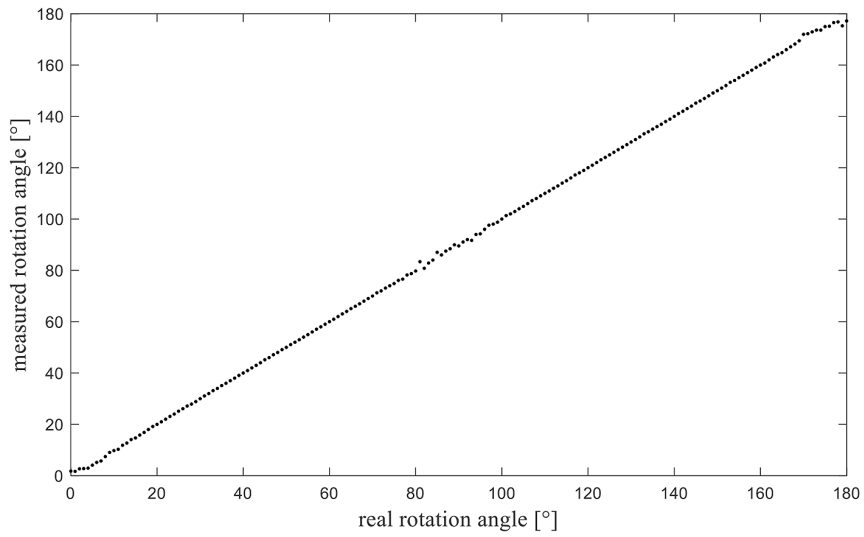


Figure 9. Measurement results for TFBG with $\theta=7^\circ$

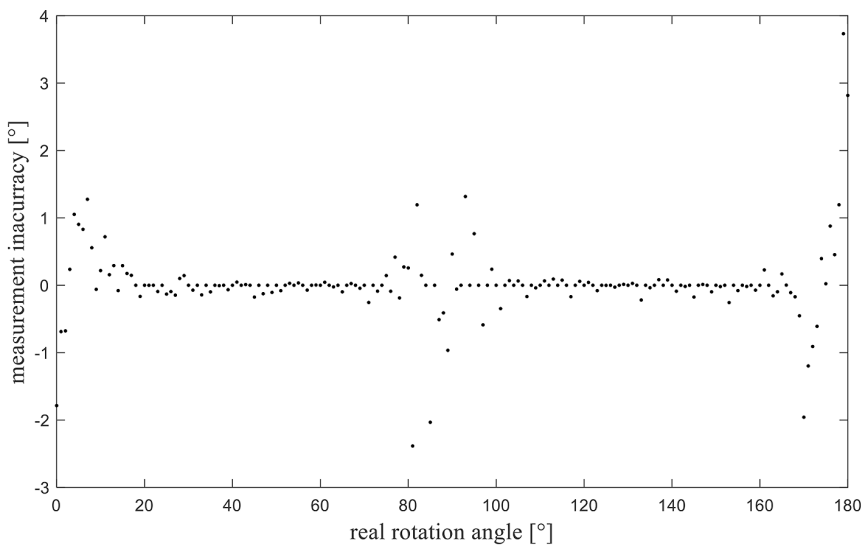


Figure 10. Measurement errors for TFBG with $\theta=7^\circ$

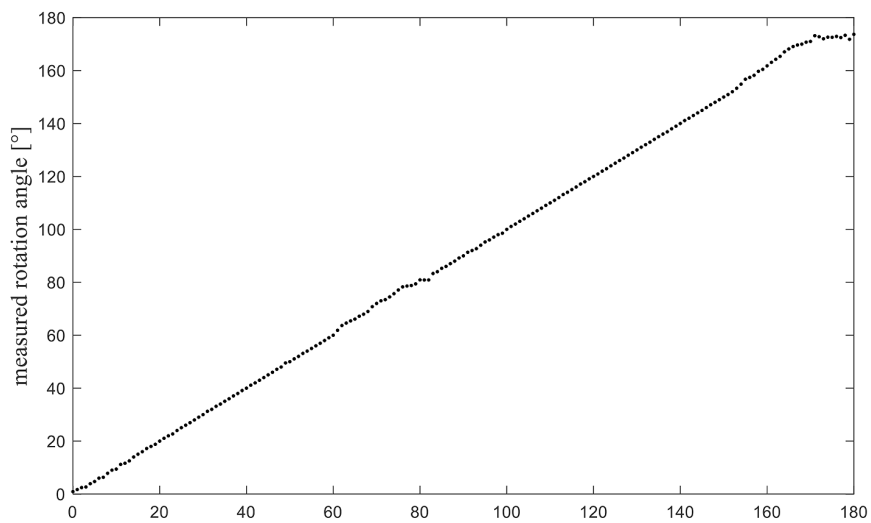


Figure 11. Measurement results for TFBG with $\theta = 5^\circ$

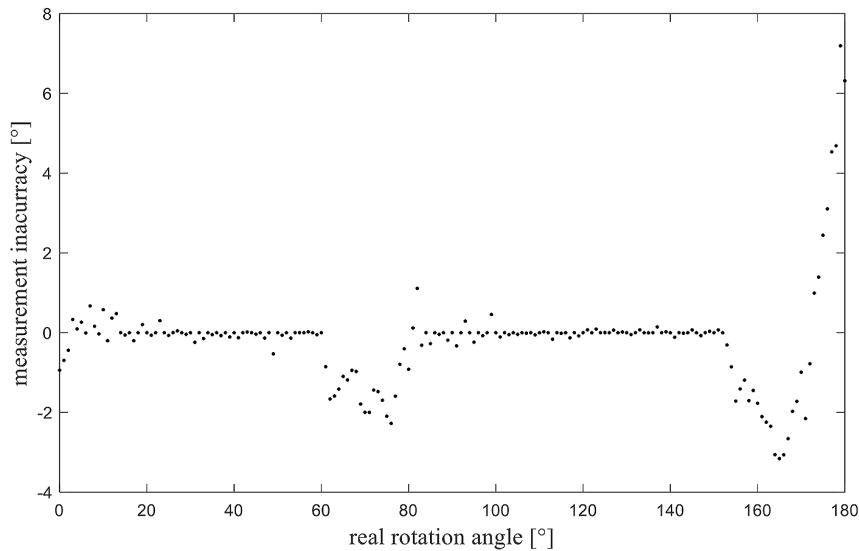


Figure 12. Measurement errors for TFBRG with $\theta = 5^\circ$

Table 1. Performance of the proposed method

Feature	Method			
	[22]	[23]	[24]	Proposed method
Possibility of distinguishing ranges 0–90 and 90–180	no	no	yes	yes
Offered precision	no data	no data	1,5°	1,1°
measurement mechanism	power measurement	power measurement	spectrum analysis with Fourier transform	spectrum analysis with DWT transform
Measurement range [°]	25–65	0–90	0–180	0–180
Method automatization	not necessary	not necessary	no	yes

plane have not been sufficiently investigated. The works [22, 23] are pioneering reports indicating the possibility of measuring the rotation angle of the light polarisation plane by analysing the power of light transmitted at specific wavelengths. Unfortunately, these methods only work over a narrow range of rotation angles. The practical feasibility of such a measurement, let alone its accuracy, has also not been investigated. Advanced analysis has been used in the method presented in [24]. A fragment of the cladding modes of the light spectrum is analysed by investigating changes in the values of selected Fourier transform coefficients. On this base, the rotation angle is calculated. The problem of the method mentioned is the necessity of experienced operator participation in the calibration process. The solution presented in this work fixes the problem by full automatization of the calibration process. Moreover, the accuracy offered by the proposed method is 26% higher and the measurement is possible over the full range of 0-180 degrees. A

summary of the main features of the compared methods is presented in Table 1.

CONCLUSIONS

The measurement of the light polarisation plane rotation angle is a poorly explored area. The present work is an important contribution to its development. The method proposed offers the highest accuracy of those presented so far. It uses the DWT, which offers great potential for signal analysis. The measurement is based on the multiple coefficients analysis which results in good accuracy. Furthermore, it introduces full automatization of the calibration process. The proposed algorithms select the optimal DWT coefficients to use. This selection is made possible through a novel method for assessing the noise of the value series. In addition, an independent measurement method operating in the 82–98 rotation angle range is proposed. This is the range in which all

analysed methods of measuring the angle of light polarisation plane rotation have reduced precision or do not allow measurement at all.

The proposed combination of methods allows measurements in the range of 0–180 to be made with an accuracy of 1.1° using a grating with a tilt of 7° . The problem of low measurement accuracy for angles close to 90° has been partially solved, but the accuracy achieved is lower than for other rotation angles. The authors plan to continue research to improve the accuracy of the examined measurement. Previous research has used optical fibres operating in the third transmission window and the wavelength of light used in the measurements was adjusted to this. The current plan is to use optical fibres, that allow light transmission at other wavelengths, obtained by doping the core with various types of ions or introducing nanocrystals [30, 31].

Acknowledgements

The research leading to these results has received funding from the commissioned task entitled “VIA CARPATIA Universities of Technology Network named after the President of the Republic of Poland Lech Kaczyński” under the special purpose grant from the Minister of Education and Science, contract no. MEiN/2022/DPI/2575, as part of the action “In the neighborhood - inter-university research internships and study visits.”

REFERENCES

1. Rovera A., Tancau A., Boetti N., Dalla Vedova M.D.L., Maggiore P., Janner D. Fiber optic sensors for harsh and high radiation environments in aerospace applications. *Sensors* 2023; 23(5), 2512.
2. Song N., Xu X., Zhang Z., Gao F., Wang X. advanced interferometric fiber optic gyroscope for inertial sensing: A Review. *Journal of Lightwave Technology* 2023; 41(13), 4023–4034. <https://doi.org/10.1109/JLT.2023.3260839>.
3. Skorupski K., Harasim D., Panas P., Ciężczyk S., Kisała P., Kacejko P., Mroczyk J., Wydra M. Overhead transmission line sag estimation using the simple opto-mechanical system with fiber bragg gratings-part 2: Interrogation System. *Sensors* 2020; 9(20), 1–21. <https://doi.org/10.3390/s20092652>.
4. Torbus S.A. Zastosowanie światłowodów telekomunikacyjnych G.652, G.653 i G.655 w polarymetrycznych czujnikach napięcia prądu. *Pomiary Automatyka Kontrola* 2011; 57(5), 441–446. (in Polish)
5. Marzejon M., Karpienko K., Mazikowski A., Jędrzejewska-Szczerska M. Fibre-optic sensor for simultaneous measurement of thickness and refractive index of liquid layers. *Metrology and Measurement Systems* 2019; 26(3), 561–568. <https://doi.org/10.24425/mms.2019.129584>.
6. Wang Y., Li B., Liu P., Hao F. Fiber-optic communication method applied to high-temperature environment. *Semiconductor Lasers and Applications XI* 2021; 1189104. <https://doi.org/10.1117/12.2602245>.
7. Dai G., Su D., Qiao X. Sensitivity-enhanced high-pressure sensor based on suspended fiber-optic fabry-pérot interferometer. *IEEE Transactions on Instrumentation and Measurement* 2022, 71, 1–7. <https://doi.org/10.1109/TIM.2022.3217847>.
8. Leal A., Díaz C., Frizera A., Lee H., Nakamura K., Mizuno Y., Marques C. Highly sensitive fiber-optic intrinsic electromagnetic field sensing. *Advanced Photonics Research* 2020; 2(1), 2000078. <https://doi.org/10.1002/adpr.202000078>.
9. He X., He Z., Ran Z., Cui J., Wang N., Gong J., Guo J., Xiao Y., Sun D., Zhu J., Li Z., Yu Y., Sun Z., Rao Y. Temperature-insensitive Quasi-distributed Fiber-optic Fabry-Perot High-pressure sensing based on microwave interference system. *Optics and Laser Technology* 2023; 161, 109069. <https://doi.org/10.1016/j.optlastec.2022.109069>.
10. Pickrell G., Udd E., Du H. Applications for fiber optic sensing in the upstream oil and gas industry. *Fiber Optic Sensors and Applications XII* 2015, 9480, 94800D. <https://doi.org/10.1117/12.2176226>.
11. Baldwin C.S. Brief history of fiber optic sensing in the oil field industry. *SPIE Fiber Optic Sensors and Applications XI* 2014, 9098. <https://doi.org/10.1117/12.2050550>.
12. Nieoczym A., Drozd K., Wójcik A. Geometric optimization of a beam detector for a wim system. *Advances in Science and Technology Research Journal* 2018; 12(3), 233–241. <https://doi.org/10.12913/22998624/97296>.
13. Stępnik P., Kisała P. Analysis of the inadequacy of determining the spectral characteristics of optical fibre periodic structures by way of numerical modelling. *Metrology and Measurement Systems* 2020; 27(1), 33–50. <https://doi.org/10.24425/mms.2020.131713>.
14. Świrniak G. Non-invasive measurements of transparent fibres. *Metrology and Measurement Systems* 2020; 27(1), 19–31. <https://doi.org/10.24425/mms.2020.131714>.
15. Hong L., Wang J.Y., Cai J.X., Teng Y.T., Qiu Z.C. Substrate-type sensitized FBG temperature sensor. *Sensor Review* 2023; 43(2), 83–91. <https://doi.org/10.1108/SR-03-2022-0156>.
16. Hegde G., Himakar B., Rao S., Hegde G., Asokan

- S. Simultaneous measurement of pressure and temperature in a supersonic ejector using FBG sensors. *Measurement Science and Technology* 2022; 33(12), 125111. <https://doi.org/10.1088/1361-6501/ac8a0a>.
17. Kisała, P. Physical foundations determining spectral characteristics measured in bragg gratings subjected to bending. *Metrology and Measurement Systems* 2022; 29(3), 573–584. <https://doi.org/10.24425/mms.2022.142275>.
 18. Harasim, D. Temperature-insensitive bending measurement method using optical fiber sensors. *Sensors and Actuators A– Physical* 2021; 332(2), 13207. <https://doi.org/10.1016/j.sna.2021.113207>.
 19. Jean-Ruel H., Albert J. Recent advances and current trends in optical fiber biosensors based on tilted fiber Bragg gratings. *TrAC Trends in Analytical Chemistry* 2024; 174, 117663. <https://doi.org/10.1016/j.trac.2024.117663>.
 20. Butov O.V., Tomyshev K.A., Nechepurenko I.A., Dorofeenko A.V., Nikitov S.A. Tilted fiber Bragg gratings and their sensing applications. *Reviews of Topical Problems* 2022, 65(12), 1290–1302. <https://doi.org/10.3367/UfNe.2021.09.039070>.
 21. An G., Liu L., Hu P., Jia P., Zhu F., Zhang Y., Liu J., Xiong J. Probe type TFBG-excited SPR fiber sensor for simultaneous measurement of multiple ocean parameters assisted by CFBG. *Optics Express* 2023, 31(3), 4229–4237. <https://doi.org/10.1364/OE.481948>.
 22. Harasim D., Kusambayeva N. The optical measurement method for structural twist monitoring with using tilted Bragg grating sensor. *Przegląd Elektrotechniczny* 2018; 94(7), 62–95. <https://doi.org/10.15199/48.2018.07.15>.
 23. Kisała P., Skorupski K., Ciężczyk S., Panas P., Klimek J. Rotation and twist measurement using tilted fibre Bragg gratings. *Metrology and Measurement Systems* 2018; 25(3), 429–440. <https://doi.org/10.24425/123893>.
 24. Kozieł G., Harasim D., Dziuba-Kozieł M., Kisała P. Fourier transform usage to analyse data of polarisation plane rotation measurement with TFBG sensor. *Metrology and Measurement Systems* 2024; 31(2), 10.24425/mms.2024.149698.
 25. Kozieł, G. Simplified Steganographic Algorithm Based on Fourier Transform. *Advanced Science Letters* 2014; 20(2), 505–509. <https://doi.org/10.1166/asl.2014.5322>.
 26. Armaselu, A. New spectral applications of the fourier transforms in Medicine, biological and biomedical fields. *Fourier Transforms – High-Tech Application and Current Trends* 2017, 235–252. <https://doi.org/10.5772/66577>.
 27. Szmajda M., Chyliński M., Szacha J., Mrocza J. Three methods for determining respiratory waves from ECG (Part I). *Metrology and Measurement Systems* 2023; 30(4), 821–837. <https://doi.org/10.24425/mms.2023.147956>.
 28. Sahoo G.R., Freed J.H., Srivastava M. Optimal wavelet selection for signal denoising. *IEEE Access* 2024; 12, 45369–45380. <https://doi.org/10.1109/ACCESS.2024.3377664>.
 29. Powroźnik P., Czerwiński D. Spectral methods in Polish emotional speech recognition. *Advances in Science and Technology Research Journal* 2016; 10(32), 73–81. <https://doi.org/10.12913/22998624/65138>.
 30. Dorosz D., Kochanowicz M., Valiente R., Diego-Rucabado A., Rodríguez F., Siñeriz-Niembro N., Espeso J.I., Lesniak M., Miluski P., Conzendorf S., Posseckardt J., Liao Z. Jimenez G.L., Müller R., Lorenz M., Schwuchow A., Leich M., Lorenz A., Wondraczek K., Jäger M. Pr³⁺-doped YPO₄ nanocrystal embedded into an optical fiber. *Scientific Reports* 2024, 14, 7404. <https://doi.org/10.1038/s41598-024-57307-4>.
 31. Kochanowicz M., Markiewicz, J. Broadband near-infrared emission in barium gallo-germanate glasses co-doped with bismuth, chromium and erbium ions. *Photonics Letters of Poland* 2024; 16, 1–3. <https://doi.org/10.4302/plp.v16i1.1247>.